Retinal OCT Image Segmentation Using Fuzzy Histogram Hyperbolization and Continuous Max-Flow

Bashir I. Dodo, Yongmin Li, and Xiaohui Liu
Department Of Computer Science
Brunel University
Uxbridge, United Kingdom
Bashir.Dodo@brunel.ac.uk, Yongmin.Li@brunel.ac.uk, XiaoHui.Liu@brunel.ac.uk

***Abstract*—The segmentation of retinal layers is vital for tracking progress of medication and diagnosis of various eye diseases. To date many methods for the analysis exist, however the speckle noise and shadows of retinal blood vessel remains a challenge, with negative influence on the performance of segmentation algorithms. Previous attempts have been focused on image pre-processing or developing sophisticated models for segmentation to address this problem, but it still remains an area of active research. In this paper we propose a simple yet efficient and computationally inexpensive method by using fuzzy histogram hyperbolization for enhancement technique, and continuous max-flow for segmentation of four retinal layers (Inner Limiting membrane, Retinal Nerve Fibre Layer, Outer segment and the Retinal Pigment Epithelium). The results show improvement in segmentation performance.**

***Index Terms*—Retinal OCT, Fuzzy Histogram Hyperbolization, Speckle Noise, Graph-Cut, Continuous Max-Flow.**

I. Introduction

Image enhancement is a necessary step for many image processing problems. The primary objective of enhancing an image is to generate a new image more suitable for further processing [1]. Because the visibility of image features is directly affected by contrast, the intelligibility of images can most often be enhanced using an appropriate transformation, especially when images occupy small part of the dynamic range [2]. It is well known that the pre-processing step affects image analysis. Image noise reduces the visibility of region of interest. In Optical Coherence Tomography (OCT) images, two main kinds of noise exists i.e the speckle noise during acquisition and the shadows of blood vessels. In handling these issues, a number of techniques have been proposed to solve these issues with varying success rates, however, the same way no universal algorithm exists for segmentation, none exists for pre-processing. Most image denoising processes are quite sensitive to the choice and fine tuning of various parameters [3].

Therefore, one of the objectives of the study is to propose an image enhancement technique of the OCT images utilizing the Fuzzy Histogram Hyperbolization (FHH) with the intention of obtaining better segmentation of the retinal structures. The segmentation of various layers of the retina is vital for tracking progress of medication and diagnosing various ocular diseases, in particular for Diabetic Retinopathy, Glaucoma and Age Related Macula Degeneration (AMD). This is especially intriguing as they are not noticed early enough by the patient, and usually cause irreversible impairment. For example, the shrinking of the Retinal Nerve Fibre Layer (RNFL) is used used in the diagnosis of glaucoma. The overall thickness of the retina (from Inner Limiting Membrane(ILM) to Retinal Pigment Epithelium(RPE)) is also used in the diagnosis of ocular diseases. Our aim is to propose a segmentation algorithm to aid with the diagnosis. This paper is organized as follows. In Section II, we provide a review of the speckle noise and how to deal with it in retinal OCT images, together with the FHH and the graph-cut method. Section III describes the proposed method, which is subdivided into two: the first part contains the enhancement technique and the later presents the segmentation method. Section IV presents experimental results on 95 OCT B-scan images and discussion. Finally conclusions are drawn in Section V.

II. Background

A. Noise and Noise Handling in Retinal OCT

Almost all OCT image analysis methods in the literature deploy a pre-processing step prior to performing any main processing steps [4]. Speckle noise in OCT images causes difficulty in the precise identification of the boundaries of layers or other structural features in the image either through direct observation or use of segmentation algorithms [4] [5]. The noise that corrupts OCT images is non-Gaussian, multiplicative and neighbourhood correlated. Thus, it cannot be easily suppressed by standard software denoising methods [6]. We can therefore say it is tradition in image analysis to enhance the image before running analysis on it. In most cases, even though the segmentation algorithms are designed to handle uncertainties and noise [7], [8], [5] , the pre-processing is used as a first step to handling the noise, irrespective of whether the analysis to be performed is in 2D [9]–[11] or 3D [8], [12]–[14], where the first step is de-noising. This is

used to remove the speckle noises and enhance the contrast between layers (usually with 3D anisotropic diffusion method, 3D median filter, 3D Gaussian filter or 3D wavelet transform) as reported in [8]. Previous attempts including spatial and frequency compounding techniques have been used to address the problem of speckle noise in OCT [15], [16] . However, the tolerance or adaptability of these techniques are quite limited, which then complicates the analysis stage.

On the other hand, a number of digital filters have been used for speckle suppression on OCT images, such as median filtering, wavelet-based filtering that employs nonlinear thresholds, anisotropic diffusion filtering [17] , and nonlinear anisotropic filtering [18]. While most of these methods are effective in reducing speckle noise, some of them tend to blur the structural boundaries in the OCT image. As a matter of fact, most of these algorithms use a defined filter window to estimate the local noise variance of a speckle image and perform the individual unique filtering process. The result is generally a reduced speckle level in areas that are homogeneous. But the image is either blurred or over smoothed due to losses in detail in non-homogeneous areas like edges or lines. Clearly, the primary goal of noise reduction is to remove the noise without losing much detail contained in an image [3]. We propose a a method, that preserves the edge information, and improve the visibility, which consequently improves performance of the segmentation method, and makes our method applicable, for diagnosis and tracking medication progress of ocular diseases

B. Fuzzy Histogram Hyperbolization(FHH)

According to the concept of fuzzy set theory [19], a mathematical framework for image processing problems can be established [20]. An image *I* can be represented with the following equation [21]:

$$I = \bigcup_{m}^{M} \bigcup_{n}^{N} \frac{\mu_{mn}}{g_{mn}} \tag{1}$$

Where g_{mn} represents the intensity of the mn^{th} pixel and μ_{mn} its membership value, given m= 1,2,3. . .M and n = 1,2,3. . .N. in line with this, using the linear index of fuzziness, the image fuzziness can be calculated with [22] :

$$\gamma(I) = \frac{2}{MN} \sum_{i=1}^{N} \sum_{j=1}^{M} min[\mu_I(g_{ij}), \bar{\mu}_I(g_{ij})] \tag{2}$$

In which $\mu_I(g_{ij})$ is the membership function of grey level g_{ij} and $\bar{\mu}_I(g_{ij})$ = 1 - $\mu_I(g_{ij})$. Fuzzy image enhancement is done by mapping image grey level intensities into a fuzzy plane using membership functions, the membership functions are modified for contrast enhancement, and the fuzzy plane is mapped back to image grey level intensities. The aim is to generate an image of higher contrast than the original image by giving the larger weight to the grey levels that are closer to the mean grey level of the image than to those that are farther from the mean.

The concept of histogram and fuzzy histogram hyperbolization was described in [23], and in [24] a method of calculating membership value for each grey level is presented as:

$$\mu(g_{mn}) = \frac{g_{mn} - g_{min}}{g_{max} - g_{min}} \tag{3}$$

where the maximum and minimum intensity values are represented by g_{max} and g_{min} respectively [19]. Then β as a fuzzifier and the desired number of grey levels L, are used to calculate the new grey values of image using the following transformation [24] :

$$g'_{mn} = (\frac{L-1}{e^{-1}-1}) * [e^{-U(g_{mn})^{\beta}} - 1] \tag{4}$$

Fuzzy histogram hyperbolization is simple and straight forward, yet effective to a range of image and signal processing applications [25].

C. Graph-Cut Segmentation

The segmentation of retinal layers has been an area of active research and has drawn a large number of researches, since the introduction of OCT [26]. Various methods have been proposed, some with focus on number of layers, others on the computational complexity, graph formulation and mostly now optimization approaches. in this regard [27] developed a multi-step approach. However the results obtained were highly dependent on the quality of image and the alterations induced by retinal pathologies. A 1-D edge detection algorithm using the Markov Boundary Model [28], which was later extended by [29] to obtain the optic nerve head and RNFL. Seven layers were obtained by [11] using a peak search interactive boundary detection algorithm based on local coherence information of the retinal structure. The Level Set method was used by [10], [12], [30], [31], which were computationally expensive compared to other optimization methods. Graph based methods in [9], [32]–[37] have reported successful segmentation results. However, the methods could still be improved, in addition to new information been discovered on the data

Graph cut is an optimal method used in solving many image processing and computer vision problems, as first observed by [38], where the problem is considered as a graph. A graph G is a pair (ν, ε) consisting of a vertex set ν (referred to as nodes in 2D or Vertex 3D nested grid) and an edge set $\varepsilon \subset \nu$ x ν. There are two main terminal vertices, the source s and the sink t.The edge set comprises of two type of edges: the spatial edges $en = (r, q)$, where $r, q \in \nu \backslash \{s \setminus t\}$, stick to the given grid and link two neighbour grid nodes r and q except s and t; the terminal edges or data edges, i.e. $e_s = (s, r)$ or $e_t = (r, t)$, where $r \in \nu \backslash \{s \setminus t\}$, link the specified terminal s or t to each grid node p respectively. Each edge is assigned a cost $C(e)$, assuming all are non-negative i.e. $C(e) \geq 0$. a cut partitions the image into two disjount sets of s and t, also termed the s-t cut. it divides the spatial grid nodes of Ω into disjoint groups, whereby one belongs to source and the other belongs to the sink, such that

$$\nu = \nu_s \bigcup \nu_t, \nu_s \bigcap \nu_t = \emptyset$$

We then introduce the concept of Max-flow/min-cut [39], where for each cut, an energy is defined as the sum of the costs C(e) of each edge e $\in \varepsilon_{st} \subset \varepsilon$, where its two end points belong to two different partitions. Hence the problem of min-cut is to find two partitions of vertices such that the corresponding cut-energy is minimal:

$$\min_{\varepsilon_{st} \subset \varepsilon} \sum_{e \in \varepsilon_{st}} C(e) \tag{5}$$

while on the other hand the max-flow is used to calculate the maximal flow allowed to pass from the source s to the sink t, and is formulated by:

$$\max_{p_s} \sum_{v \in \nu \setminus \{s,t\}} p_s(v) \tag{6}$$

In the spatially continuous setting, let Ω be a closed spatial 2-D or 3-D domain and s, t be the source and sink terminals. At each point x $\in \Omega$ the flow passing x is denoted by p(x); the directed source flow from s to x by $p_s(x)$; and the directed sink flow from x to t by $p_t(x)$.
To calculate the max flow we take; For each x $\in \Omega$ let $p_s(x)$ $\in \mathbb{R}$ denote the flow from the source s to x and $p_t(x) \in \mathbb{R}$ denote the flow from x to the sink t. Define further the vector field p : $\Omega \longmapsto \mathbb{R}^n$ as the spatial flow within Ω, where n is the dimension of the image domain Ω. The flows p(x), $p_s(x)$, $p_t(x)$ are constrained by the capacities $C(x)$,$C_s(x)$ and $C_t(x)$ as follows:

$$\begin{aligned} |p(x)| &\leq c(x), & \forall x \in \Omega \\ p_s(x) &\leq c_s(x), & \forall x \in \Omega \\ p_t(x) &\leq c_t(x), & \forall x \in \Omega \\ divp(x) - ps(x) + pt(x) &= 0, & a.ex \in \Omega \end{aligned}$$

Here div p evaluates the total incoming spatial flow locally around x. subject to the above constraints, the continous max-flow is formulated as :

$$\sup_{p_s, p_t, p} \{P(p_s, p_t, p) = \int_{\Omega} p_s(x) dx\} \tag{7}$$

III. The Proposed Method

We first enhance the images using the FHH to promote homogeneity and suppress the noise, then segment the retinal layers using the continuous max-flow algorithm.

A. Enhancement

There are a number of operations that could be performed with membership modification, determined by the value of β termed the fuzzifier, for example dilation or concentration if β = 0.5 or 2 respectively. By selection of a specific membership function the fuzzy hyperbolization can be used for segmentation and edge detection [23], as the value of β approaches 0, the results are similar to that of histogram equalization, whereas if β approaches values 5 and above, it tends to provide result similar to segmentation. Samples are shown in Fig. 1, where the global FHH is used, with values β= 0.3 and 5.

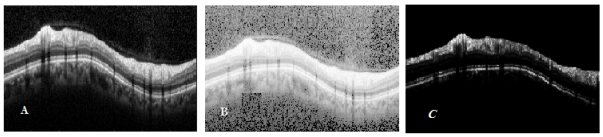

Fig. 1. Examples of transformation using A-unprocessed image; B- β= 0.3; and C- $\beta = 5$

We therefore take two main things into consideration: i) Most image denoising processes are quite sensitive to the choice and fine tuning of various parameters [3]. ii) The fuzzifier β modifies the membership values additionally, and so, the gray level dynamics of the resulting image can be changed [23]. In this regard, we propose a window (threshold), whereby the value of β is within that threshold. From 4:

$$g'_{mn} = (\frac{L-1}{e^{-1}-1}) * [e^{-U(g_{mn})^{\beta}} - 1]$$

we can now limit β with the following constraint:

$$T_{min} \leq \beta \leq T_{max} \tag{8}$$

Where T_{min} and T_{max} are the minimum acceptable values of β. To achieve the above, we introduce constant *C*, which can be called the stabilizer, used in keeping the value of β within the set threshold, this in turn means the below condition is applied to determine and set the value of β :

$$\begin{aligned} &\beta = \beta + C \\ &\beta = T_{min} \quad if \quad \beta + C < T_{min} \\ &\beta = T_{max} \quad if \quad \beta + C > T_{max} \end{aligned} \tag{9}$$

Of course the threshold values can always be adjusted easily, for the method to adapt to a wider range of images and applications of fuzzy sets, however, we limit our study to the enhancement of retinal OCT images to suppress and handle speckle noise and blood vessel interference. after the transformation, the image is enhanced and this has positive effect in calculating the flow.

B. Segmentation

We adopt the unsupervised image segmentation [40]. For image segmentation without user inputs, a piecewise constant function is used as the image model: where two gray values f_1 and f_2 are chosen priori for clues to build data terms:

$$C_s(x) = D(f(x)f_1(x)), \quad C_t(x) = D(f(x)f_2(x)) \tag{10}$$

where $D(\cdot)$ is some penalty function. By utilizing the augmented Lagrangian method [41] the max-flow function can be represented as follows:

$$\begin{aligned} Lc(P_s, P_t, P, \lambda) = &\int_{\Omega} p_s dx + \int_{\Omega} \lambda(divp - p_s + p_t) dx \\ &- \frac{c}{2} \|divp - p_s + p_t\|^2 \end{aligned} \tag{11}$$

Where λ is the Lagrangian multiplier introduced to optimize the flow and c is the steps in augmented Lagrangian. A condition is imposed whereby only saturated flows contribute to the total spatial flows and cuts, therefore for $p^*(x)$:

$$C_{TV}^{\alpha} = \{p | \|p\|_{\infty} \leq \alpha, p_n | \partial\Omega = 0\} \tag{12}$$

where α is the penalty parameter to the total variation term $\partial\Omega$ and is constant through out. In other words, at potential cut locations x $\in \Omega$ where $\nabla\lambda^*(x) \neq 0$ the spatial flow $p^*(x)$ is saturated, while at locations x $\in \Omega$ where $|p(x)| < \alpha$ is unsaturated we must have $\nabla\lambda^*(x) = 0$ and therefore the cut does not sever the spatial domain at x. This allows the optimization and the labeling to be carried out simultaneously. Then an iterative process is employed to optimize the flows and the multiplier until convergence, where in each iteration K^{+1} the convergence criterion is calculated by

$$err^k = \|\lambda^{k+}1\lambda^k\| / \|\lambda^{k+1}\| \tag{13}$$

where err^* is the error rate. Set the starting values p_s^1, p_t^1, p^1 and λ^1, let k = 1 and start k^{th} iteration. Optimizing p by fixing other variables

$$\begin{aligned} p^{k+1} &= arg \max_{\|p\|\infty \leq \alpha} Lc(p_s^k, p_t^k, p, \lambda^k). \\ &= arg \max_{\|p\|\infty \leq \alpha} -\frac{c}{2}\|divp(x) - F^k\|^2 \end{aligned} \tag{14}$$

where $\prod_{\alpha}$ is the convex projection onto the convex set $C_{\alpha} = q \mid\mid\mid q \mid\mid \leq \alpha$ and F^k is a fixed variable. The above problem (14) is then computed by:

$$p^{k+1} = \prod_{\alpha} p^k + c\nabla(divp^k - F^k) \tag{15}$$

Optimizing p_s by fixing other variables

$$\begin{aligned} p_s^{k+1} &= arg \max_{p_s(x) \leq C_s(x)} Lc(p_s, p_t^k, p^{k+1}, \lambda^k) \\ &= arg \max_{p_s(x) \leq C_s(x)} \int_{\Omega} p_s dx - \frac{c}{2}\|p_s - G^k\|^2 \end{aligned} \tag{16}$$

where G^k is a fixed variable and optimizing ps we compute at each x $\in \Omega$ pointwise. Optimize p_t by fixing other variables:

$$\begin{aligned} p_t^{k+1} &= arg \max_{p_t(x) \leq C_t(x)} Lc(p_s^{k+1}, p_t, p^{k+1}, \lambda^k) \\ &= arg \max_{p_t(x) \leq C_t(x)} -\frac{c}{2}\|p_t - H^k\|^2 \end{aligned} \tag{17}$$

where H^k is a fixed variable and optimizing pt can be simply solved by

$$p_t(x) = \min(H^k(x), C_t(x)) \tag{18}$$

Finally update λ by:

$$\lambda^{k+1} = \lambda^k - c(divp^{k+1}p_s^{k+1} + p_t^{k+1}) \tag{19}$$

Further details with respect to the augmented Lagrangian, total variation and Lipschitz principles used in the method can be obtained from [42] [43] [44] [41].

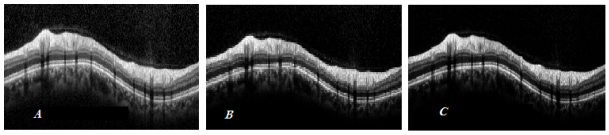

Fig. 2. Visual comparison of methods. A: unprocessed image. B: enhancement using Fuzzy Type-2 [20]. C: our method.

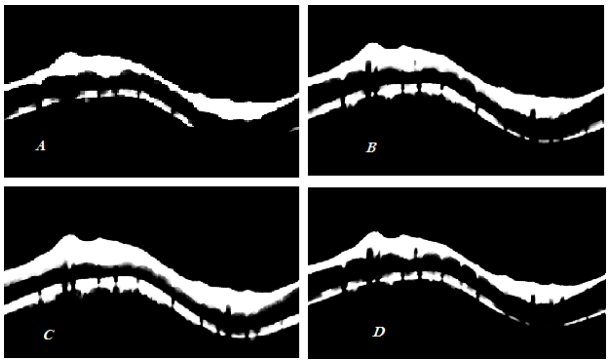

Fig. 3. Segmentation results of four retinal layers. A: the ground truth image. B: result without any enhancement. C: Fuzzy Type-2 [20]. D: the proposed method.

IV. Results and Discussions

The algorithm was tested on a dataset of 95 OCT macular scans of size 341x695. For visual comparison purpose, we show the enhanced images using the fuzzy type-2 [20] and the proposed method in Fig. 2, and the results of the segmentation of for retinal layers in Fig.3, because it is not ideal to rely on visual comparison only, and usually images are enhanced or pre-processed to allow better analysis. Our method produces better results using the enhancement method proposed in this paper. We then carry out further validation on the segmentation result using four criteria for the evaluation purpose i.e. accuracy, sensitivity, specificity and precision, and compare the results using: Raw image (unenhanced), Type-2 Fuzzy [20] and the proposed method. Details of results are shown in Table I, where AC, SE, SP, and PR refer to Accuracy, sensitivity, specificity and Precision respectively.

These measurements are computed with the following equa-

TABLE I
Evaluation Table

Method	AC	SE	SP	PR
Raw image	0.8992	0.8750	0.8028	0.7121
Type-2 Fuzzy [20]	0.9286	0.9228	0.8636	0.8846
Our Method	0.9651	0.9547	0.9183	0.9163

tions:

$$Accuracy = \frac{TP + TN}{(TP + FP + FN + TN)}$$
$$Sensitivity = \frac{TP}{(TP + FN)}$$
$$Specificity = \frac{TN}{(TN + FP)}$$
$$Precision = \frac{TP}{(TP + FP)}$$

where TP, TN, FP and FN refer to true positive, true negative, false positive and false negative respectively. TP represents the number of pixels which are part of the region that are labeled correctly by both the method and the ground truth. TN represents the number of pixels which are part of the background region and labeled correctly by both the method and the ground truth. FP represents the number of pixels labeled as a part of the region by the method but labeled as a part of the background by the ground truth. Finally, FN represents the number of pixels labeled as a part of the background by the system but labeled as a part of the region in ground truth, additional information can be obtained from [45] .

Both methods are tested on a dataset of 95 B-scan OCT images. For all experiment with the proposed method C = 1.5, T_{min}=1.8 and T_{max} = 2.3, α = 0.4, c = 0.3, err^* = $1e^{-4}$ and maximum iteration is set to 200 though the method converges before 80 iterations for most images. We consider the value of β to be obtained from calculation and then stabilized (in place of constant), as that is an indicator as to what end of the threshold is more applicable to the particular image.

There are a number of methods used in calculating β, however for our data they provide low fuzziness result, ranging from $\sim$0.34$-$0.75, and that is the importance of the stabilizer. The value of β is directly proportional to the value of C in this case, where the range of the threshold is easily obtainable, to keep the transformation within the desired operation context and obtain better results. Our method also outperforms the method proposed in [20], in addition to the ability to incorporate information user observes or holds on a dataset.

We introduce the stabilizer C, to allow the input of prior knowledge, and in turn this gives more usability and simplicity. This can be interpreted or related to the interactive graph-cut [42] concept, where a user is given the option of selecting seeds based on his image and allow the algorithm to perform the computation. Now if the results are unsatisfactory, the user can easily change the seeds to obtain better results. However, in our case as mentioned in section III, all parameters i.e. β, C and threshold window are adjustable, and this can be obtained easily by a single test experiment, to determine what value range is suitable for a particular dataset. The value of this is to provide the ability to incorporate more prior information in order to guide the method during computation.

V. Conclusions

We have developed a method to segment multiple retinal layers from OCT images using the Fuzzy Histogram Hyperbolization and continuous max-flow, thus enabling the separate computation of individual layer properties, such as thickness. Unlike other pre-processing techniques such as Gaussian, median filter and average filters etc., the proposed enhancement method has an advantage that it conserves the edges.Therefore it can be used solely, or as an enhancement step, before filtering or smoothing. A drawback is the use of constant for the stabilizer, for which it might be improved to adapt to an even wider dataset without the need for much initialization. High segmentation accuracy has been achieved in the experiments and the overall process is applicable in real time as it converges within 4-8seconds, as both steps are computationally inexpensive. The proposed method adapts to inconsistency in retinal structures and can therefore be used in diagnosis of visual impairments and tracking progress of medication.

Acknowledgement

The authors would like to thank Djibril Kaba, Khalid Eltayef and Chuang Wang for the informative discussions and for providing the dataset and its ground-truth labels.

References

[1] A. Mokrane, "A New Image Contrast Enhancement Technique Based on a Contrast Discrimination Model," *CVGIP: Graphical Models and Image Processing*, vol. 54, no. 2, pp. 171–180, 1992.

[2] W. Frei, "Image enhancement by histogram hyperbolization," *Computer Graphics and Image Processing*, vol. 6, no. 3, pp. 286–294, 1977.

[3] H. M. Salinas and D. C. Fernandez, "Comparison of PDE-based nonlinear diffusion approaches for image enhancement and denoising in optical coherence tomography," *IEEE Transactions on Medical Imaging*, vol. 26, no. 6, pp. 761–771, 2007.

[4] R. Kafieh, H. Rabbani, and S. Kermani, "A review of algorithms for segmentation of optical coherence tomography from retina," *J Med Signals Sens*, vol. 3, no. 1, pp. 45–60, 2013.

[5] A. Mishra, A. Wong, K. Bizheva, and D. A. Clausi, "Intra-retinal layer segmentation in optical coherence tomography images." *Optics Express*, vol. 17, no. 26, pp. 23 719–28, 2009.

[6] M. A. Mayer, J. Hornegger, C. Y. Mardin, and R. P. Tornow, "Retinal Nerve Fiber Layer Segmentation on FD-OCT Scans of Normal Subjects and Glaucoma Patients." *Biomedical optics express*, vol. 1, no. 5, pp. 1358–1383, 2010.

[7] H. Bogunović, M. D. Abràmoff, and M. Sonka, "Geodesic graph cut based retinal fluid segmentation in optical coherence tomography," *Proceedings of the Ophthalmic Medical Image Analysis (OMIA 2015), Held in Conjunction with MICCAI 2015*, pp. 49–56, 2015.

[8] Z. Wang, M. Jenkins, G. Linderman, H. Bezerra, Y. Fujino, M. Costa, D. Wilson, and A. Rollins, "3-D Stent Detection in Intravascular OCT Using a Bayesian Network and Graph Search." *IEEE transactions on medical imaging*, vol. 0062, no. c, pp. 1–14, 2015.

[9] D. Kaba, Y. Wang, C. Wang, X. Liu, H. Zhu, a. G. Salazar-Gonzalez, and Y. Li, "Retina layer segmentation using kernel graph cuts and continuous max-flow." *Optics express*, vol. 23, no. 6, pp. 7366–84, 2015.

[10] C. Wang, D. Kaba, and Y. Li., "Level set segmentation of optic discs from retinal images," *Journal of Medical Systems*, vol. 4, no. 3, pp. 213–220, 2015.

[11] D. Cabrera Fernández, H. M. Salinas, and C. A. Puliafito, "Automated detection of retinal layer structures on optical coherence tomography images." *Optics Express*, vol. 13, no. 25, p. 10200, 2005.

[12] C. Wang, Y. Wang, and Y. Li, "Automatic choroidal layer segmentation using markov random field and level set method," *IEEE journal of biomedical and health informatics*, 2017.

[13] C. Wang, Y. Wang, D. Kaba, Z. Wang, X. Liu, and Y. Li., "Automated layer segmentation of 3d macular images using hybrid methods," in *Proc. International Conference on Image and Graphics. Tianjing, China.*, vol. 9217, 2015, pp. 614–628.

[14] C. Wang, Y. Wang, D. Kaba, H. Zhu, Z. Wang, X. Liu, and Y. Li., "Segmentation of intra-retinal layers in 3d optic nerve head images," in *Proc. International Conference on Image and Graphics. Tianjing.*, vol. 9219, 2015, pp. 321–332.

[15] N. Iftimia, B. E. Bouma, and G. J. Tearney, "Speckle reduction in optical coherence tomography by path length encoded angular compounding," *Journal of Biomedical Optics*, vol. 8, no. 2, pp. 260–263, 2003.

[16] M. Pircher, E. Gotzinger, R. Leitgeb, A. F. Fercher, and C. K. Hitzenberger, "Speckle reduction in optical coherence tomography by frequency compounding," *Journal of Biomedical Optics*, vol. 8, no. 3, pp. 565–569, 2003.

[17] D. Fernandez, "Delineating fluid-filled region boundaries in optical coherence tomography images of the retina," *IEEE Transactions on Medical Imaging*, vol. 24, no. 8, pp. 939–945, 2005.

[18] G. Gregori and R. Knighton, "A Robust Algorithm for Retinal Thickness Measurements using Optical Coherence Tomography (Stratus OCT)," *Investigative Ophthalmology & Visual Science*, vol. 45, no. 13, p. 3007, may 2004.

[19] L. A. Zadeh, "Fuzzy Set," *Information and Control*, vol. 8, pp. 338–353, 1965.

[20] P. Ensafi and H. Tizhoosh, "Type-2 fuzzy image enhancement," *Image Analysis and Recognition*, vol. 3656, pp. 159–166, 2005.

[21] K. G., H. R. Tizhoosh, T. Lilienblum, C. J. Moore, and B. Michaelis, "Fuzzy Image Enhancement and Associative Feature Matching in Radiotherapy," in *IEEE international Conference on Neural Networks*, 1997, p. 1490.

[22] H. R. Tizhoosh, "Fuzzy Image Processing: Potentials and State of the Art," *International Conference on Soft Computing*, vol. 1, no. February, pp. 321–324, 1998.

[23] H. R. Tizhoosh and M. Fochem, "Fuzzy histogram hyperbolization for image enhancement," *Proceedings EUFIT*, vol. 95, no. January 1995, 1995.

[24] H. R. Tizhoosh, G. Krell, and B. Michaelis, "Locally Adaptive Fuzzy Image Enhancement," *Image (Rochester, N.Y.)*, vol. 1, no. 1, pp. 1–5.

[25] V. Magudeeswaran and C. G. Ravichandran, "Fuzzy Logic-Based Histogram Equalization for Image Contrast Enhancement," *Mathematical Problems in Engineering*, 2013.

[26] D. Huang, E. A. Swanson, C. P. Lin, J. S. Schuman, W. G. Stinson, W. Chang, M. R. Hee, T. Flotte, K. Gregory, and C. A. Puliafito, "Optical coherence tomography." *Science (New York, N.Y.)*, vol. 254, no. 5035, pp. 1178–81, 1991.

[27] M. Baroni, P. Fortunato, and A. La Torre, "Towards quantitative analysis of retinal features in optical coherence tomography." *Medical engineering & physics*, vol. 29, no. 4, pp. 432–441, 2007.

[28] D. Koozekanani, K. Boyer, and C. Roberts, "Retinal thickness measurements from optical coherence tomography using a Markov boundary model," *IEEE Transactions on Medical Imaging*, vol. 20, no. 9, pp. 900–916, 2001.

[29] K. L. Boyer, A. Herzog, and C. Roberts, "Automatic recovery of the optic nervehead geometry in optical coherence tomography," *IEEE Transactions on Medical Imaging*, vol. 25, no. 5, pp. 553–570, 2006.

[30] J. Novosel, K. A. Vermeer, G. Thepass, H. G. Lemij, and L. J. V. Vliet, "Loosely Coupled Level Sets For Retinal Layer Segmentation In Optical Coherence Tomography," *IEEE 10th International Symposium on Biomedical Imaging*, pp. 998–1001, 2013.

[31] C. Wang, Y. Wang, D. Kaba, Z. Wang, X. Liu, and Y. Li, "Automated Layer Segmentation of 3D Macular Images Using Hybrid Methods," *Image and Graphics*, vol. 9217, pp. 614–628, 2015.

[32] T. Zhang, Z. Song, X. Wang, H. Zheng, F. Jia, J. Wu, G. Li, and Q. Hu, "Fast retinal layer segmentation of spectral domain optical coherence tomography images," *Journal of Biomedical Optics*, vol. 20, no. 9, p. 096014, 2015.

[33] A. Salazar-Gonzalez, D. Kaba, Y. Li, and X. Liu, "Segmentation of the blood vessels and optic disk in retinal images," *IEEE journal of biomedical and health informatics*, vol. 18, no. 6, pp. 1874–1886, 2014.

[34] A. G. Salazar-Gonzalez, Y. Li, and X. Liu, "Retinal blood vessel segmentation via graph cut," in *International Conference on Control Automation Robotics & Vision*, 2010, pp. 225–230.

[35] A. Salazar-Gonzalez, Y. Li, and X. Liu, "Automatic graph cut based segmentation of retinal optic disc by incorporating blood vessel compensation," *Journal of Artificial Intelligence and Soft Computing Research*, vol. 2, no. 3, pp. 235–245, 2012.

[36] M. Haeker, X. Wu, M. Abràmoff, R. Kardon, and M. Sonka, "Incorporation of regional information in optimal 3-D graph search with application for intraretinal layer segmentation of optical coherence tomography images." *Information processing in medical imaging : proceedings of the ... conference*, vol. 20, pp. 607–618, 2007.

[37] M. K. Garvin, M. D. Abràmoff, X. Wu, S. R. Russell, T. L. Burns, and M. Sonka, "Automated 3-D intraretinal layer segmentation of macular spectral-domain optical coherence tomography images." *IEEE transactions on medical imaging*, vol. 28, no. 9, pp. 1436–1447, 2009.

[38] A. Seheult, D. Greig, and B. Porteous;, "Exact Maximum A Posteriori Estimation For Binary Images," *Journal of the Royal Statistical Society*, vol. Vol. 51, no. No. 2, pp. 271 –279, 1989.

[39] L. R. Ford and D. R. Fulkerson, "Maximal flow through a network," *Journal canadien de mathématiques*, vol. 8, pp. 399–404, 1956.

[40] J. Yuan, E. Bae, X.-C. Tai, and Y. Boykov, "A study on continuous max- flow and min-cut approaches," *2010 IEEE Conference*, vol. 7, pp. 2217–2224, 2010.

[41] D. P. Bertsekas, *Nonlinear programming*. Athena scientific Belmont, 1999.

[42] Y. Boykov and M.-P. Jolly, "Interactive Graph Cuts for Optimal Boundary & Region Segmentation of Objects in N-D Images," *Proceedings Eighth IEEE International Conference on Computer Vision. ICCV 2001*, vol. 1, no. July, pp. 105–112, 2001.

[43] Y. Boykov and V. Kolmogorov, "An experimental comparison of min-cut/max- flow algorithms for energy minimization in vision," *IEEE Transactions on Pattern Analysis and Machine Intelligence*, vol. 26, no. 9, pp. 1124–1137, 2004.

[44] V. Kolmogorov and R. Zabih, "What Energy Functions Can Be Minimized via Graph Cuts?" *IEEE Transactions on Pattern Analysis and Machine Intelligence*, vol. 26, no. 2, pp. 147–159, 2004.

[45] A. Fenster and B. Chiu, "Evaluation of segmentation algorithms for medical imaging," in *Engineering in Medicine and Biology Society, 2005. IEEE-EMBS 2005. 27th Annual International Conference of the*. IEEE, 2005, pp. 7186–7189.